Experimental Investigation of Airway Pressures in Human Airway Models with Compliant Components

Marcin Buchajczyk[1], Patrick Geoghegan[1], Natalia Kabaliuk[1], Cletus Adams[1], Callum Spence[2] and Mark Jermy[1]

[1]Department of Mechanical Engineering
University of Canterbury, Private Bag 4800, Christchurch 8041, New Zealand

[2]Fisher & Paykel Healthcare Limited
15 Maurice Paykel Place, East Tamaki, Auckland 2013, PO Box 14 348, Panmure, Auckland 1741, New Zealand

Abstract

A new manufacturing process to construct a human airway model with key complaint components was developed. Experimental analysis was then performed with the results compared to that of a rigid model to investigate the influence that soft tissues had on airway pressures during natural and nasal high flow therapy (NHFT) assisted breathing and investigate the validity of previous rigid wall assumptions in experimental investigation. The airway geometry was obtained from CT scan data and 3D printing technology was used to fabricate the anatomically correct polymer model. A soft silicone was used to simulate the compliance of the tongue, soft palate and vocal fold regions. Breathing was simulated in both the rigid and compliant model using a computer controlled pulsatile pump. The results revealed that the compliant airway model experienced different static pressures during both natural and NHFT assisted breathing. Natural breathing results showed similar oscillatory pressure profiles between compliant and rigid airways, however the compliant airway had larger pressures on peak expiration and lower pressures on peak inspiration at the velopharynx and oropharynx regions. With the application of NHFT at 30 L/min, the compliant airway had greater pressures than the rigid airway for both breathing phases, upstream of the site of compliance. Below the soft palate, only peak expiratory pressures were affected. At NHFT at 60 L/min, the compliant airway pressures were greater than their corresponding rigid pressures for both breathing phases, at all regions.

Introduction

Breathing therapy devices are widely used to tackle various respiratory complications. Nasal High Flow Therapy (NHFT), delivers body temperature and pressure saturated (BTPS) air via a nasal cannula at constant flow rates that can range from 10-60 L/min. This is a novel therapy and its mechanisms of action are not completely understood, however, several have been hypothesised [4] including: dead space washout of the airway cavity [13], leading to improvement of gas exchange; and elevation of airway pressure in both adults [6, 9] and infants [8], which can support alveolar recruitment in diseased patients.

In-vitro studies have used anatomically correct airway models to investigate the efficacy of NHFT [3, 11, 14]. Due to the materials used in fabricating these polymer models, the studies assumed completely rigid airways. The current study used a life-size, semi-flexible open mouth airway model to scrutinize the rigid airway assumption. The model simulated compliance of the tongue, soft palate and the vocal fold regions by matching the elasticity of these tissues. The tissue models were designed as removable inserts and two sets of these tissue components were made: a 3D printed rigid set, to simulate the original, rigid models; and a silicone cast set, which simulated the compliance of the relevant tissues. These inserts were interchangeable and hence the same airway model could simulate a rigid or partially compliant boundary condition.

Method

Segmentation/airway extraction

Accurate airway models can be produced using patient specific geometries based on computed tomography (CT) scan data. Image segmentation is the process of grouping pixels based on their intensity and therefore can be used to identify the airway passages in the CT slices. An intensity threshold was set in 3DSlicer (https://www.slicer.org/) to discriminate between tissue and air, and hence an airway geometry (Figure 1 left) was segmented and extracted from the CT data [5].

The airway surface was extruded uniformly to create a model of thickness of 2 mm. The tongue, soft palate and vocal fold soft tissue regions were cleared from the airway model to create cavities where these components could be inserted. A female mating interface was designed to allow for a press fit fastening between the airway and the insertable components. The model was separated into two halves on the sagittal plane to allow access for fitting the insertable components. A flange was projected around the airway model in the same plane to accommodate for screw clearances as the two halves were fastened with bolts (Figure 1 right). Pressure taps were incorporated at specific regions along the airway that allowed for pressure probes to measure static pressures.
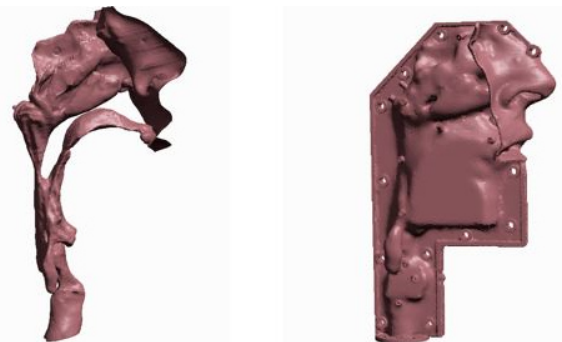

Figure 1. Segmented airway geometry (left) and digital airway model prepared for printing (right).

Insert Design

Geometries for the soft palate, tongue and vocal fold tissue simulants were produced using the segmentation method. Insert geometry was the same for both rigid and compliant components. The geometries required further editing from the segmented extracts, such as adding a male mating interface so it could be secured in the airway model. Figure 2 shows the transition from extracted soft palate geometry to the modified insert design. The tongue and the vocal fold components had similar modifications.

Figure 2. Raw soft palate component (left) and digital model of final soft palate component (right).

The airway model (Figure 5) and the rigid tissue inserts (Figure 3) were printed on a Projet HD 3000 Plus photopolymer jetted 3D printer with a printing accuracy of 25 – 50 μm. A layer thickness of 29 μm was used to produce a smooth finish with the acrylic printing material (Visijet EX200). The support material was wax.
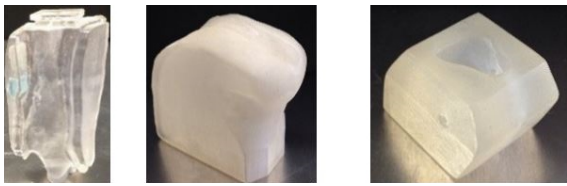

Figure 3. 3D printed rigid inserts: Soft palate (left), tongue (center) and vocal folds (right).

Material Selection for Soft Tissue Components

Compliance for the tongue, the soft palate and vocal fold models was simulated by using a material which matched the reported elasticity of the corresponding tissues [1, 2]. The chosen material for the simulants was silicone A-341, a two part, platinum cured RTV silicone soft gel. A previous study by Kashif et al. [7] defined its elasticity when mixed with varying compositions of thinning oil (Dow Corning 50cst) to match breast tumour stiffness. This was used to find a composition that replicated the relevant tissue elasticity (Table 1).

Tissue	Tissue Elasticity	Silicone Composition
Soft Palate	7.4 kPa	45.60 %
Tongue	7.74 kPa	46.40 %
Vocal Fold	4.57 kPa	38.80 %

Table 1. Elastic properties of internal soft tissues and the required silicone composition (by weight) to match the corresponding elasticity.

Soft Tissue Moulds

Anatomically accurate sacrificial moulds were 3D printed for casting the body of the soft tissue simulants, by FDM printing in ABS plastic on a Stratasys Elite printer. The silicone was injected into the mould and after curing was complete, the moulds were bathed in acetone for 4- 6 hours, removing the ABS layer, leaving only the silicone model. Once all visible ABS was dissolved, the compliant components were removed and fixed to rigid frames, which were part of the respective anatomical geometry and provided mating into the airway. Figure 4 shows the final compliant tongue and soft palate inserts.

Figure 4. Compliant tongue (left) and soft palate (right) tissue inserts. These have a rigid frame on the exterior, which is part of the tissue anatomy.

Experimental Setup

Once complete, the airway model was attached to a benchtop experimental setup, which simulated respiration in the airway model. The airway model was orientated in the supine position and was attached to a pulsatile pump at the tracheal end via tubing. The pump drove air in and out of the model, and replicated the physiological flow pattern of respiration as programmed in LabView [14]. The model had NHFT administered via an Optiflow™ nasal cannula and Airvo™ humidifier, provided by Fisher & Paykel Healthcare. The airflow was quantified with static pressure measurements, and were recorded at the tap locations in the airway with AMS 5915 differential pressure sensors at a sampling rate of 25 Hz. An endoscopic camera was used to observe deformation in the compliant inserts during testing, which was inserted in the airway through the tracheal outlet of the model.

Assembling and Sealing

A gasket was applied between the airway halves (Figure 5) to prevent any leaks in the model. Air flow was applied into the trachea and flow rate was recorded once a pressure of 400 Pa was achieved as this was the largest pressure measured in previous studies [3]. This was repeated with all outlets blocked and a ratio of the flow rates gave a leak rate fraction. The gasket gave a maximum leak rate of 2.5 % and was deemed suitable for this study.

Figure 5. 3D printed airway model. Shown is one airway half with rigid inserts (left) and the completely assembled airway (right).

Results and Discussion

Static pressures were measured along the pharynx for a completely rigid airway and a compliant soft palate airway model. This was carried out for natural breathing and NHFT assisted breathing at 30 L/min and 60 L/min flow rates. The lung flow rate set by the piston motion was the same in all cases. Figure 7 to Figure 9 show the results as a phase averaged breath cycle with error bars of one standard deviation from 5 test repetitions. The paper discusses the pressures measured at the velopharynx (VP) and oropharynx (OP) (Figure 6), as these regions were representative of the superior and inferior sites of compliance, respectively.

The static pressure results during natural breathing (Figure 7) showed that the compliant airway followed a similar trend to the rigid airway, however compliant pressures were lower on peak inspiration and higher at peak expiration. At peak inspiration in the VP region, the pressure in the compliant airway had a reduction of 3.8 % relative to the corresponding rigid peak-to-peak pressure profile, and at peak expiration compliant model pressures were greater by 7.7 %. It can be seen that compliance affected the OP region more, particularly on peak inspiration. The peak inspiratory pressure had a reduction of 21.4 % and the peak expiratory pressure was greater by 6.3%. Pirnar et al. [10] used computational methods to study the compliant soft palate during closed mouth breathing. They found that the VP region would reduce and

increase in cross-sectional for inspiration and expiration, respectively. Their compliant model had lower pressures on both expiration and inspiration, which was not consistent with this experiment and may be attributed to the difference in breathing modes. There may be more dramatic effects seen in closed mouth breathing as more air flows through the VP region due to the single path of flow, compared to open mouth breathing where the flow is branched into oral and nasal paths. It is hypothesised that the compliant soft palate in the current model tended toward the posterior of the airway due to the influence of gravity on the supine orientated airway model. This would increase the resistance in these regions and cause pressures to be lower on peak inspiration and greater on peak expiration.

Experiments with NHFT at 30 L/min, resulted in compliant static pressures at the VP to be greater than the rigid pressures for both breathing phases (Figure 8). This corresponded to an increase of 8.5% and 15.2% at peak inspiration and peak expiration, respectively. The OP region in the compliant airway had a peak inspiratory pressure that resembled its relative rigid pressure with a reduction of only 2 %, and on peak expiration it had an increase of 13.3 %. Endoscopic imaging revealed that the inferior tip of the soft palate (uvula) would move toward the anterior of the airway on expiration. This motion would increase the cross-sectional area in the airway channel at the VP region thus decelerating the flow and elevating the pressure at this site. As the material of the soft palate was incompressible, a deformation that caused widening on one side of the soft palate would cause a narrowing of the opposite side. It is likely that the deformation of the uvula would also cause the passage between the pharynx and mouth to constrict. Spence [12] showed with particle image velocimetry that all air is expired through the oral cavity during open mouth breathing with NHFT of 30 L/min; therefore on expiration, both the VP and OP sites were upstream of the flow exiting through the oral cavity on expiration. A constriction of the passage between pharynx and oral cavity would cause a resistance to the airway sites upstream of this site, resulting in elevation of expiratory pressures at both sites.

The compliant airway experienced greater peak inspiratory pressures in the VP region, compared to the rigid airway at the same site, with an increase of 8.5 % at the peak. At the OP region, the peak inspiratory compliant pressure was similar to its corresponding rigid pressure with a reduction of 2.1%. It is hypothesised that the jet from the NHFT therapy caused a widening in the VP, where the soft palate tissue is located. This would explain the elevation in inspiratory pressures at the VP when comparing to its rigid counterpart, as the flow velocity would decelerate and pressure would increase. However, this could not be confirmed with the endoscope as its limited field of view only showed the movements of the uvula.

NHFT at 60 L/min (Figure 9) resulted in compliant pressures that were greater than the rigid pressures for the entire breath cycle at both sites. The compliant airway had an increase in peak inspiratory pressure of 21.4 % and 11.8 % at the VP and OP sites, respectively, and at peak expiration, these were greater by 33.8 % and 27.8 % at the VP and OP sites, respectively. Endoscopic imaging showed motion similar to the 30 L/min case with more pronounced movement. The increase in expiratory pressures for the compliant airway can be explained by the same mechanisms described for NHFT 30 L/min expiration, however, greater pressure rises were observed due to the increased level of therapy used. Tuft flow visualization at the mouth showed that air exited from the mouth at both breathing phases. Assuming that NHFT increases cross-sectional at the VP region on inspiration for a compliant airway, it can also be assumed that this would greater for higher NHFT flows. This would result with a narrowing of the passage between the pharynx and oral cavity, and would restrict airflow exiting the mouth on inspiration. This would explain the elevation in pressures on inspiration in the compliant airway.
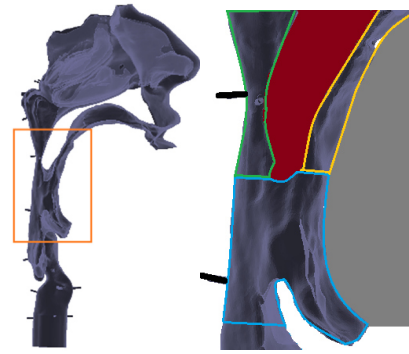

Figure 6. Airway region of interest showing VP (green), OP (blue), tongue (grey), soft palate (red), oral cavity (yellow), pressure tap location (black).
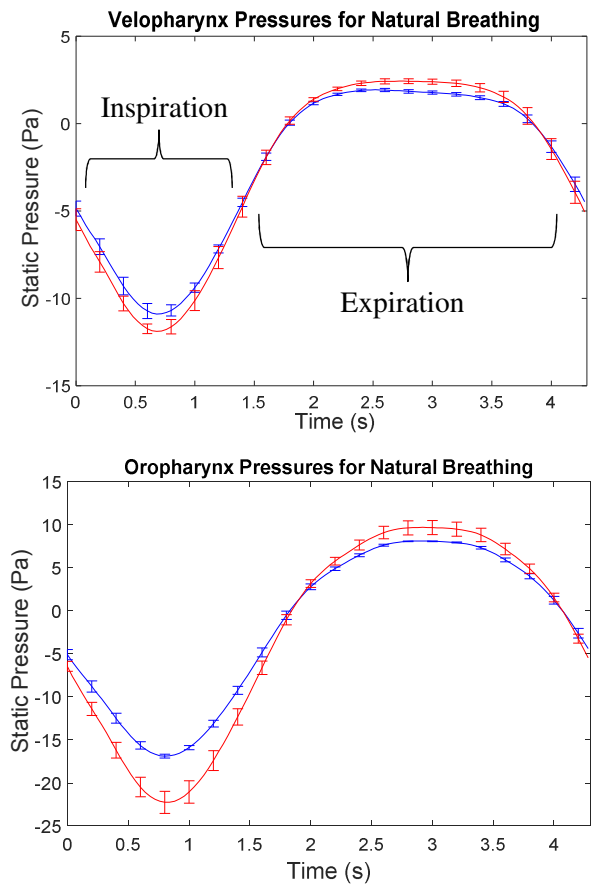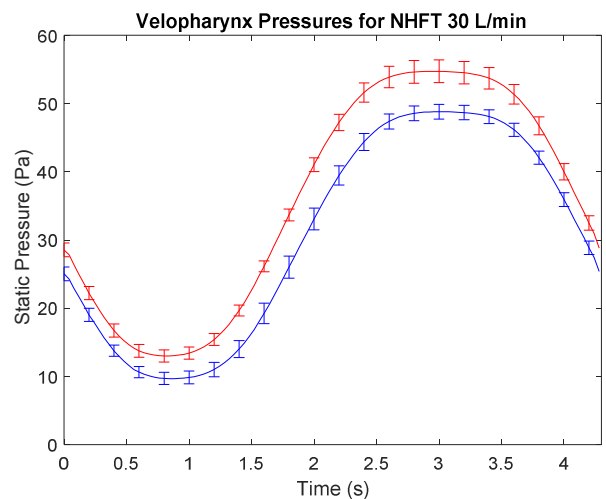

Figure 7. Static pressure profiles for compliant soft palate (red) airway and rigid airway (blue) in VP (top) and OP (bottom) for natural breathing.
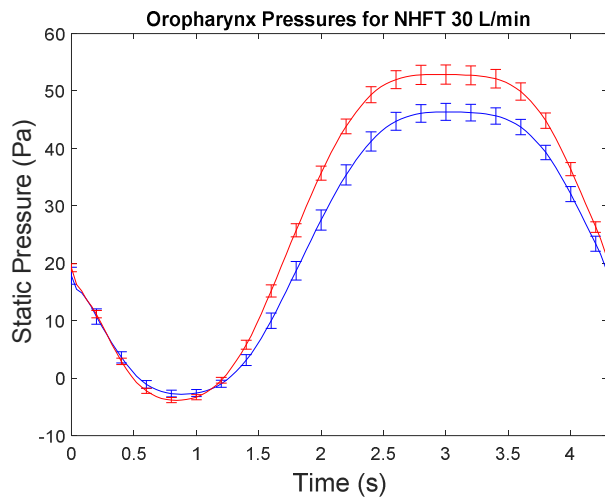
Figure 8. Static pressure profiles for compliant soft palate airway (red) and rigid airway (blue) in VP (top) and OP (bottom) for NHFT 30 L/min.
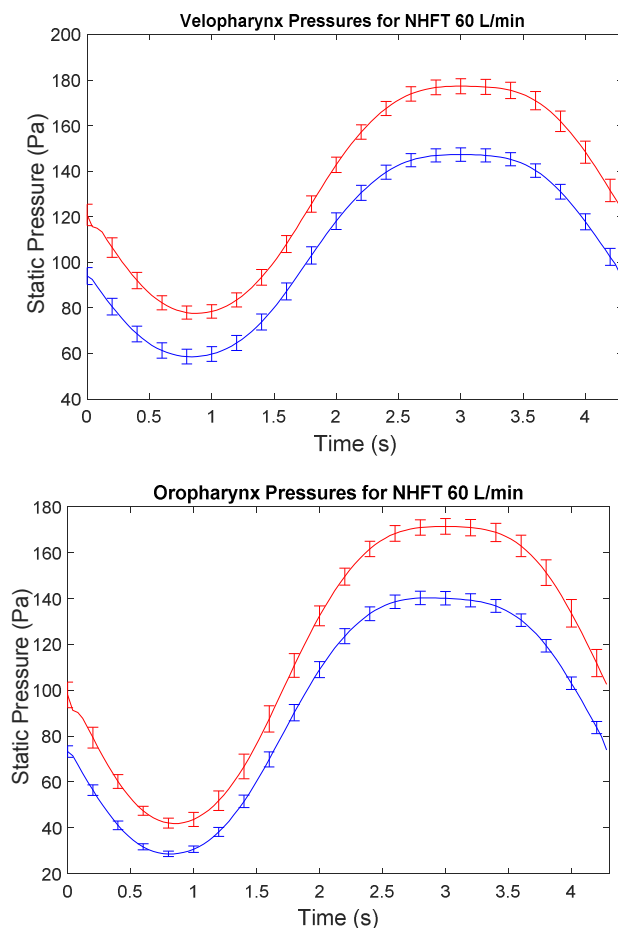

Figure 9. Static pressure profiles for compliant soft palate airway (red) and rigid airway (blue) in VP (top) and OP (bottom) for NHFT 60 L/min.

Conclusion

A compliant airway model was manufactured using silicone compositions which mimicked physiological tissue stiffness'. The model was designed to interchange between compliant and rigid, to draw comparison between the two cases. A test with a compliant soft palate adapted to the model revealed that compliance did affect the airway pressures, and the extent would increase with the addition of greater NHFT flows. Endoscopic imaging revealed motion of the soft palate on expiration with NHFT assisted breathing. These effects will have influence the mechanical work of breathing and the end expiratory pressure. Further testing is required for the remaining compliant tissues. A computational study with a deformable mesh is required to further investigate the effects of compliance on NHFT assisted breathing.

References

[1] Chan, R.W., et al., *Relative contributions of collagen and elastin to elasticity of the vocal fold under tension.* Annals of biomedical engineering, 2007. **35**(8): p. 1471-1483.

[2] Cheng, S., et al., *Viscoelastic properties of the tongue and soft palate using MR elastography.* Journal of Biomechanics, 2011. **44**(3): p. 450-454.

[3] Dey, K.M., *Anatomic Dead Space Washout and Flow Effects during Breathing with Nasal High Flow Therapy.* 2014.

[4] Dysart, K., et al., *Research in high flow therapy: mechanisms of action.* Respiratory medicine, 2009. **103**(10): p. 1400-1405.

[5] Geoghegan, P.H., et al., *Fabrication of rigid and flexible refractive-index-matched flow phantoms for flow visualisation and optical flow measurements.* Experiments in Fluids, 2012. **52**(5): p. 1331-1347.

[6] Groves, N. and A. Tobin, *High flow nasal oxygen generates positive airway pressure in adult volunteers.* Australian Critical Care, 2007. **20**(4): p. 126-131.

[7] Kashif, A.S., et al., *Silicone breast phantoms for elastographic imaging evaluation.* Medical physics, 2013. **40**(6): p. 063503.

[8] Lampland, A.L., et al., *Observational study of humidified high-flow nasal cannula compared with nasal continuous positive airway pressure.* The Journal of pediatrics, 2009. **154**(2): p. 177-182. e2.

[9] Parke, R.L., M.L. Eccleston, and S.P. McGuinness, *The effects of flow on airway pressure during nasal high-flow oxygen therapy.* Respiratory care, 2011. **56**(8): p. 1151-1155.

[10] Pirnar, J., et al., *Computational fluid-structure interaction simulation of airflow in the human upper airway.* Journal of biomechanics, 2015. **48**(13): p. 3685-3691.

[11] Spence, C., N. Buchmann, and M. Jermy, *Unsteady flow in the nasal cavity with high flow therapy measured by stereoscopic PIV.* Experiments in fluids, 2012. **52**(3): p. 569-579.

[12] Spence, C.J.T., *Experimental Investigations of Airflow in the Human Upper Airways During Natural and Assisted Breathing.* 2011.

[13] Sztrymf, B., et al., *Beneficial effects of humidified high flow nasal oxygen in critical care patients: a prospective pilot study.* Intensive care medicine, 2011. **37**(11): p. 1780-1786.

[14] Van Hove, S., et al., *An Experimental and Numerical Investigation of CO_2 Distribution in the Upper Airways During Nasal High Flow Therapy.* Annals of biomedical engineering, 2016: p. 1-13.